Featured in Physics

Determining the $^3P_0$ Excited-State Tune-Out Wavelength of ^{174}Yb in a Triple-Magic Lattice

Tim O. Höhn,[1,2] René A. Villela,[1,2] Er Zu,[1,2] Leonardo Bezzo,[1,2,*] Ronen M. Kroeze,[1,2] and Monika Aidelsburger[1,2,3,†]

[1] *Fakultät für Physik, Ludwig-Maximilians-Universität, 80799 München, Germany*
[2] *Munich Center for Quantum Science and Technology (MCQST), 80799 München, Germany*
[3] *Max-Planck-Institut für Quantenoptik, 85748 Garching, Germany*

(Received 25 June 2025; accepted 3 November 2025; published 6 January 2026)

Precise state-dependent control of optical potentials is of great importance for various applications utilizing cold neutral atoms. In particular, tune-out wavelengths for the clock state pair in alkaline-earth(-like) atoms provide maximally state-selective trap conditions that hold promise for the realization of novel approaches in quantum computation and simulation. While several ground-state tune-out wavelengths have been determined, similar experimental studies for metastable excited states are challenged by inelastic collisions and Raman losses, so far prohibiting precise measurements of excited-state tune-out conditions. In this work we report on the measurement of a tune-out wavelength for the metastable $^3P_0$ clock state in ^{174}Yb at 519.920(9) THz. In order to circumvent collisional losses, we isolate individual $^3P_0$ atoms in a two-dimensional clock-magic-wavelength lattice at 759 nm. To minimize the limitation imposed by Raman scattering, we further implement resolved sideband cooling on the clock transition, which allows us to reduce the lattice depth and surpass lifetimes of 5 s. The precision of the tune-out measurement is further enhanced by fluorescence imaging in a triple-magic configuration, where we implement molasses cooling on the $^3P_1$ intercombination line and identify a magic angle of 38.5(9)° in the clock-magic lattice.

DOI: 10.1103/32q9-j82c

I. INTRODUCTION

Alkaline-earth(-like) (AEL) atoms have been utilized for a plethora of remarkable applications, from advanced quantum computation protocols [1–4] to quantum simulation of the SU(N) Fermi-Hubbard model [5–8]. In particular the ultranarrow transition to the $^3P_0$ state has enabled the development of extremely accurate optical lattice and tweezer clocks [9–13], the realization of highly entangled states for enhanced metrology [14], as well as the realization of spin-orbit coupling [15] and artificial gauge fields in synthetic dimensions [16,17]. A crucial ingredient for these results is the precise cancellation of differential ac Stark shifts in so-called magic traps [18].

However, for certain applications like site-resolved addressing [1,19,20] or the simulation of mass-imbalanced particles [21] and lattice gauge theories [22], state-selective traps constitute an invaluable resource. The extreme case of a fully vanishing atom-light coupling of one state at a tune-out wavelength, while the other state retains a finite polarizability, has been employed for erasure conversion of quantum gate errors [4], and it has been suggested to be used for simulations of twisted bilayer systems [23,24], the realization of novel quantum gates [25], and the separation into storage and transport traps for quantum processors [26,27]. Since this condition requires equal blue- and red-detuned polarizability contributions from the dominant transitions, tune-out wavelengths in alkali atoms only exist close to transitions, resulting in detrimental near-resonant scattering. For AEL atoms, the strongly decoupled transition manifolds for the ground and metastable excited state in turn result in far-detuned tune-out wavelengths and thus provide the ability to perform high-fidelity resorting operations or local lightshift applications with minimal scattering.

*Current address: ICFO - Institut de Ciencies Fotoniques, The Barcelona Institute of Science and Technology, 08860 Castelldefels (Barcelona), Spain.
†Contact author: Monika.Aidelsburger@physik.uni-muenchen.de

Published by the American Physical Society under the terms of the Creative Commons Attribution 4.0 International license. Further distribution of this work must maintain attribution to the author(s) and the published article's title, journal citation, and DOI.

Furthermore, as precise *ab initio* polarizability calculations for the $^1S_0 - {}^3P_0$ clock state pair are highly nontrivial, measurements of distinct points such as tune-out wavelengths are crucial to test and improve the accuracy of these models [30]. In this work we demonstrate the versatility of controlling the light shifts of various states by identifying a magic angle between the external magnetic field and the trapping laser's polarization [1,12,31–34] for the narrow $^1S_0 \rightarrow {}^3P_1$ cooling transition in ^{174}Yb. This enables a triple-magic condition in the clock-magic lattice at 759 nm and a precise determination of the tune-out wavelength for the $^3P_0$ clock state, where its polarizability exhibits a zero crossing.

Compared to the ground-state tune-out measurements performed in AEL atoms so far, which have been based on parametric heating schemes with long-lived ground-state atoms trapped in one-dimensional (1D) lattices [28,35], the detection of a tune-out wavelength for the metastable $^3P_0$ state is significantly challenged by several factors. First, strong inelastic collisions of nearby $^3P_0$ atoms result in fast losses [36,37], limiting Kapitza-Dirac scattering measurements using pulsed optical lattices with a Bose-Einstein condensate (BEC) [38–42]. In this paper, we inhibit collisions by confining bosonic ^{174}Yb in a two-dimensional (2D) lattice, and mitigate thermally assisted tunneling to neighboring sites via ground-state cooling on the clock transition [43]. Second, deep optical traps induce strong off-resonant Raman scattering to other internal states [29,44], such that one has to resort to shallow optical lattices to reach the sufficiently long lifetimes necessary for parametric heating measurements, as used in the present paper. Additionally, our high signal-to-noise ratio detection scheme, based on magic-angle molasses cooling during fluorescence imaging, provides the resolution to detect loss rates as low as a few millihertz.

II. EXPERIMENTAL RESULTS

The experiment starts by directly loading about 7×10^4 ^{174}Yb atoms from a magneto-optical trap (MOT) into a $\approx 140\,\mu$K deep clock-magic optical lattice at $\lambda = 759.3$ nm. Compared to our previous work, our setup has been upgraded to a three-dimensional (3D) lattice, which is used for loading and imaging of the atoms [28]. The 3D geometry consists of two orthogonal, retro-reflected and vertically polarized horizontal lattices and a shallow-angle vertical lattice as illustrated in Fig. 1(a). The 3D lattice allows us to reach total potential depths on the order of 450 μK and strong confinement in all directions. Fluorescence imaging is realized by implementing molasses cooling on the $^1S_0 \rightarrow {}^3P_1$ intercombination line [Fig. 1(b)] [1,45–47]. Since this transition is only 183 kHz wide, high-fidelity imaging relies on magic trapping [47–49]. This condition is generally not fulfilled in a clock-magic optical lattice. The finite total electronic angular momentum

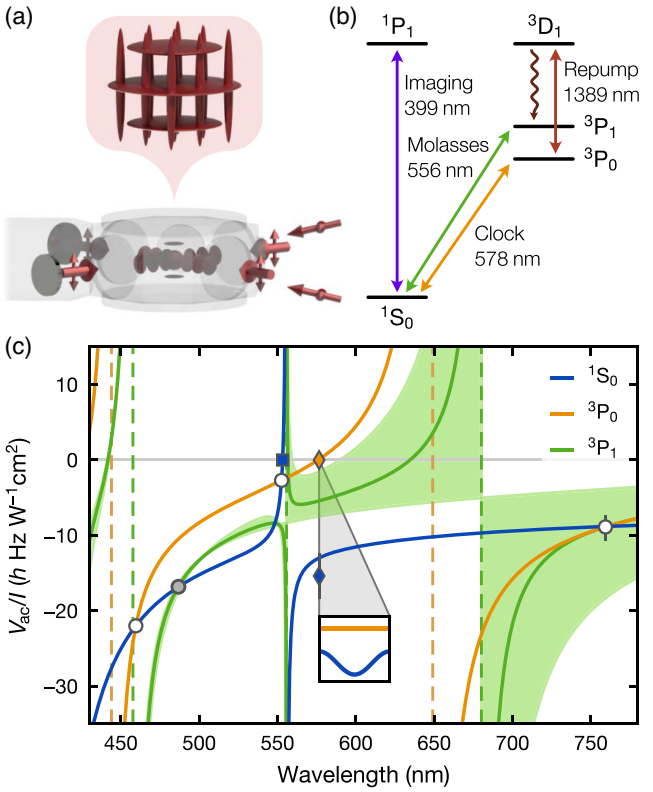


FIG. 1. Experimental setup, simplified level structure, and ac polarizabilities of ^{174}Yb. (a) Sketch of the 3D clock-magic lattice. Double-sided arrows indicate the polarization of the individual lattice beams. (b) Simplified level scheme including the clock ($^1S_0 \rightarrow {}^3P_0$), repumping ($^3P_0 \rightarrow {}^3D_1$), imaging ($^1S_0 \rightarrow {}^1P_1$) and molasses cooling transitions ($^1S_0 \rightarrow {}^3P_1$). (c) Light shifts of the three lowest-lying states in linearly polarized traps, using an empirical model (solid lines) [28,29]. The green shaded area highlights the tunability of the total $^3P_1(m_{J'} = 0)$ light shift by adjusting the angle of the external magnetic field. Round markers indicate the measured magic wavelengths ($^1S_0 \rightarrow {}^3P_0$ white, $^1S_0 \rightarrow {}^3P_1$ gray), diamonds the $^3P_0$ tune-out wavelength (orange, corresponding measured $^1S_0$ polarizability in blue) and the square marker depicts the measured $^1S_0$ tune-out wavelength. Inset: schematic trapping potential at the $^3P_0$ tune-out wavelength.

of the $^3P_1$ state, however, induces a significant tensor shift, which can be leveraged to achieve a triple-magic condition [Fig. 1(c)], as has been demonstrated for ^{171}Yb [1]. Here, one can utilize the dependence of the tensor shift on the relative angle θ between the trap polarization and the external magnetic field. In the case of ^{174}Yb, the total expected resonance shift for the Zeeman substate $m_{J'}$ in the presence of a magnetic field B can be expressed as

$$\Delta V_{\mathrm{ac}} = -\frac{I}{2c\epsilon_0}\left(\Delta\alpha_{\mathrm{s}} + \alpha_{\mathrm{t}}\frac{3\cos^2\theta - 1}{2}(3m_{J'}^2 - 2)\right) + \mu B m_{J'}, \tag{1}$$

where $\Delta\alpha_s$ is the scalar differential polarizability, α_t is the tensor polarizability of the $^3P_1$ state, $\mu = g_{J'}\mu_B$ is the magnetic moment, and μ_B is the Bohr magneton.

To determine the magic angle at 759 nm in ^{174}Yb, we perform atom loss spectroscopy on all three $m_{J'}$ transitions in a $\approx k_B \times 240\,\mu K \approx 2400\,E_{rec}$ deep 2D lattice, where k_B is the Boltzmann constant, $E_{rec} = h^2/(2m\lambda^2)$ the lattice recoil energy, h Planck's constant, and m the atomic mass. This spectroscopy is performed for various magnetic field angles relative to the vertical polarization axis at a total field of $B = 14$ G and we compare the resulting resonance positions to the case of free-space resonances to determine the light shift according to Eq. (1) [Fig. 2(a)]. The latter are determined within a short time-of-flight period during which the lattice is quenched off, while the direction and intensity of the circularly polarized spectroscopy beam is chosen such that the projection on the individual transitions is sufficiently large over the whole angle range and yields only minimally power-broadened linewidths, which we find to be the case for a beam approximately copropagating with one of the horizontal lattice arms and $I \approx I_{sat}$. This yields a magic angle for the $m_{J'} = 0$ state near 35° and further demonstrates that the differential light shift for transitions to the $m_{J'} = \pm 1$ states can be minimized using magnetic fields orthogonal to the lattice polarization.

To obtain a more precise result for the $m_{J'} = 0$ magic angle, we scan the lattice depth for various magnetic field angles. This results in linearly increasing or decreasing resonance shifts as depicted in Fig. 2(b), such that we can use the fitted slopes to obtain the zero crossing of the total light shift at $\theta_{magic} = 38.5(9)°$ [Fig. 2(c)]. Here, we make use of the vanishingly small curvature of the expected functional form in Eq. (1) and use a simple linear fit for this result. While this fit yields a statistical uncertainty on the mrad level, the reported uncertainty is governed by systematic effects, where the dominant contribution stems from the calibration of θ [29].

The magic angle facilitates fast efficient fluorescence imaging via the $^3P_1$ state by directly collecting fluorescence photons scattered by the cooling light with a high-NA objective [1]. In this work, we instead apply an additional weak probe beam of resonant 399 nm photons for imaging on the $^1P_1$ state ($I \approx 10^{-3}\,I_{sat}$) [45], which will be crucial for achieving single-site resolution in the retroreflected clock-magic lattice with a small lattice constant of only 380 nm. To counteract the resulting heating we perform molasses cooling with the horizontal MOT beams at an intensity of $I \approx I_{sat}$ and a detuning δ of approximately -20 kHz from the free-space resonance while leaving the imaging frequency unchanged [Fig. 3]. In the 3D lattice geometry, we find an overall improved loading rate from the MOT for a horizontal polarization of the vertical lattice beams, which we attribute to a larger interference contrast and, thus, a stronger vertical confinement. As a result, a simultaneous magic condition for all three lattice

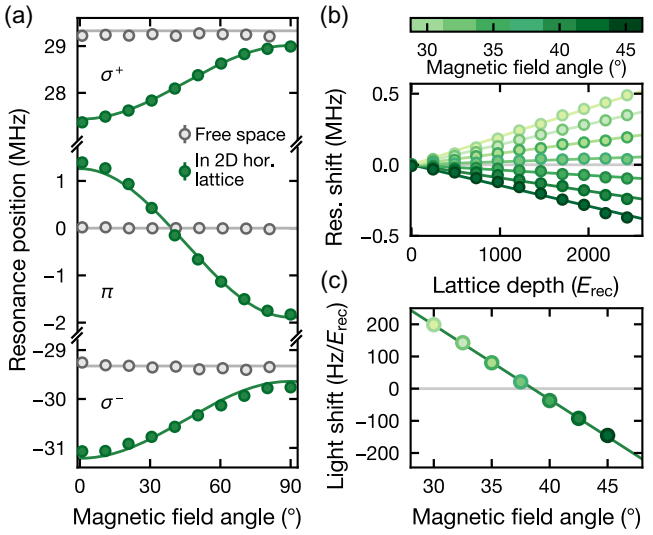


FIG. 2. Measuring the magic angle for the $^1S_0 \rightarrow {}^3P_1$ transition at 759 nm. (a) Light shifted $^1S_0 \rightarrow {}^3P_1$ σ^+, π, and σ^- transitions (green) for various magnetic field angles relative to the vertical lattice polarization, and stationary free-space resonances (gray). The solid lines correspond to a single fit to the data using Eq. (1). The error bars are obtained from the Lorentzian resonance fit uncertainty and are smaller than the datapoints. (b) Resonance shifts of the π transition for various magnetic field angles and lattice depths close to the magic angle. The data is fitted with a linear function (solid lines). (c) The fitted slopes are used to determine the magic angle $\theta_{magic} = 38.5(9)°$ using a linear fit since the curvature of the light shift in this regime is negligible.

beams cannot be achieved. Nonetheless, we observe that we can reach a near-magic condition for all three lattice beams by also adjusting the azimuthal magnetic field angle ϕ [Fig. 3(b)]. This way, we find a contour on which the total number of photon counts for a constant exposure time remains close to the maximum, indicating efficient cooling conditions. The contour can be understood as the light shift introduced by the horizontal lattice being approximately canceled by an opposite light shift from the vertical lattice, with additional effects stemming from the sizeable electric field splitting compared to the modest external magnetic field strength of 1.3 G [29]. We further note that even for a subpar field orientation a large fraction of atoms remains trapped, whereas the photon count without cooling already saturates at 10 ms due to complete scattering-induced atom loss, as can be seen in Fig. 3(c), inset. Using an exposure time of 200 ms, we can thus collect 16× more fluorescence photons per atom on the camera than without cooling, allowing us to resolve atom number variations on the order of 100 atoms.

To study the lifetime of atoms in the $^3P_0$ state, we apply a resonant, 260 μs long clock π-pulse, followed by a strong 399 nm pulse to remove all atoms that were not transferred to the metastable state and a repump pulse

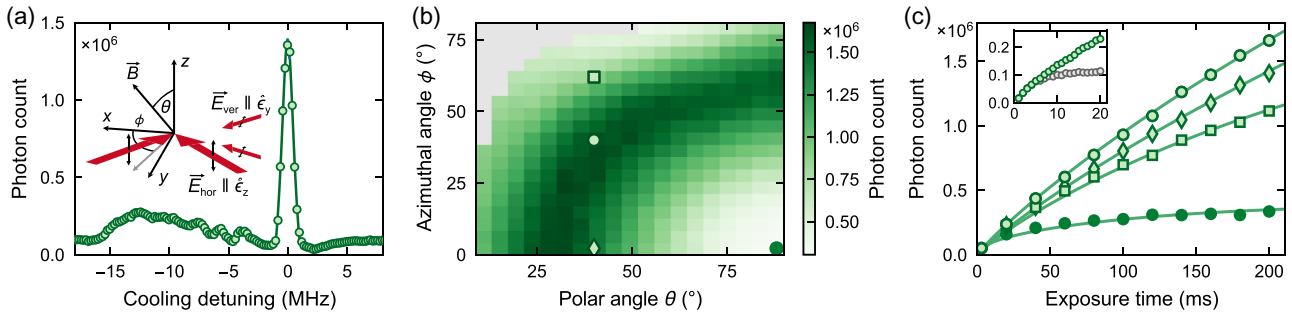


FIG. 3. Molasses cooling in a 3D lattice. (a) For a near-magic condition in a $\approx 400\,\mu$K deep 3D lattice with orthogonal polarizations of the horizontal and vertical lattices we observe a ≈ 600 kHz wide molasses resonance close to the free-space $^3P_1$ π transition leading to a strongly enhanced collection of fluorescence photons after 200 ms exposure time with weak 399 nm probe light [magnetic field orientation as indicated by the bright circle in (b)]. In contrast, the light-shifted $\sigma^{\pm}$ transitions do not allow for efficient imaging of the whole cloud. The solid line is a Lorentzian fit to the cooling resonance data. Inset: lattice beams (bright red single arrows), corresponding polarization vectors (black double-sided arrows), and magnetic field configuration. (b) Imaging efficiency for different magnetic field orientations. While it is not possible to simultaneously reach the magic angle for the horizontal and vertical lattices, the resonance linewidth enables sufficiently near-magic conditions for a broad range of B-field angles. Markers indicate the magnetic field angles used in panels (a),(c). (c) Evolution of the photon counts for varied exposure times. The near-linear dependence observed for various magnetic field directions demonstrates that the heating-induced loss by scattering of 399 nm light is efficiently counteracted. The solid lines serve as a guide to the eye. Inset: comparison to an uncooled cloud (gray) that exhibits full atom loss after approximately 10 ms.

before starting the fluorescence imaging sequence [29]. By varying the wait time between the clock-excitation and repump pulse we can therefore trace the $^3P_0$ loss rate. In contrast to the ground state, where vacuum losses are typically predominant, off-resonant Raman scattering of 759 nm trap photons limits the $^3P_0$ lifetime in deep traps [50]. Hence, the tune-out measurement has to be performed in a weak lattice to achieve the best resolution for the heating-induced excess loss rate measurements. To mitigate spilling and two-body inelastic collisions due to atoms occupying higher vibrational bands that can tunnel fast in a shallow optical lattice, we perform cooling prior to the measurement scheme described above. Since this work employs spinless, bosonic ^{174}Yb, cooling techniques that leverage the existence of multiple ground states, such as Λ-enhanced gray molasses or Raman sideband cooling [51–56], are out of reach. Instead, we utilize resolved sideband cooling on the clock transition similar to Ref. [57], which we adapt for use in a 2D lattice [29,43]. We note that horizontal cooling in a pure 2D lattice is sufficient to localize and separate the atoms well, while the third direction can remain uncooled. After clock-sideband cooling we obtain a mean motional occupation number of $\bar{n} \approx 0.1$ along each horizontal direction in a $\approx 220\,E_{\mathrm{rec}}$ deep lattice. This enhances the $^3P_0$-state lifetime to $\tau = 5.2(1)$ s, which is defined as the 1/e-decay time extracted with an exponential fit [Fig. 4(a)]. This lifetime is still limited by Raman scattering as evidenced by the substantially shorter lifetime of the $^3P_0$ state compared to that of $^1S_0$, and the crossover to a linear increase of the $^3P_0$ loss rate for deep lattices [Fig. 4(b)]. For shallow lattice depths, strong inelastic collisions and spilling losses increase the loss rate of both $^1S_0$ and $^3P_0$ states. A fraction of Raman-scattered atoms from the $^3P_0$ state reappears in the $^1S_0$ ground state by decaying via the intermediate $^3P_1$ state, while atoms scattered to the $^3P_2$ state are anti-trapped and subsequently lost. The former pathway can be detected by measuring the total atom number, i.e., by omitting from the detection sequence a dedicated resonant pulse that normally removes any $^1S_0$ atoms. The observed fraction is consistent with the results reported in Ref. [50].

As a next step, while the magic lattice remains in a 2D geometry, we superimpose a retro-reflected lattice close to the tune-out wavelength at an arbitrarily chosen angle of 30° to the 2D lattice. Sinusoidal intensity modulation of this tune-out lattice induces parametric heating, enabling us to probe the atoms' polarizability. Similar to the 1D lattice case utilized in previous experiments [28,35], the incommensurability of wavelengths then incurs mostly phase modulation for atoms in certain lattice sites, while others predominantly experience amplitude modulation as shown in Fig. 5(a), where the modulation spectrum displays two strong resonances at the longitudinal trap frequency and its first multiple. We note that a pure phase modulation from a running wave induced by two detuned beams would provide a stronger single resonance, however, at the expense of a 4 times lower peak intensity. Choosing the modulation frequency of 64 kHz that shows the strongest loss response, we study the effect of the tune-out lattice on the clock-state lifetime as a function of the laser frequency $f_{\mathrm{l}} = f_{\mathrm{to}} + \Delta$, where f_{to} is the $^3P_0$ tune-out frequency and Δ is the laser's

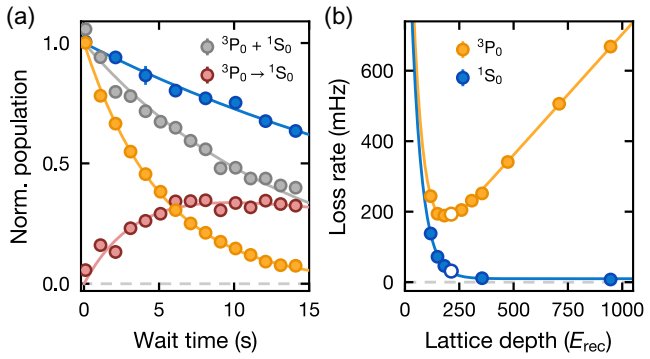


FIG. 4. $^3P_0$ clock-state lifetime. (a) Lifetime of sideband-cooled atoms in a $220\,E_{rec}$ deep 2D lattice initialized in the $^1S_0$ state (dark blue) or $^3P_0$ state (orange). Raman-scattering-induced losses out of $^3P_0$ partially reappear in the $^1S_0$ state and can be detected from the total atom number (gray) via the difference to the $^3P_0$ decay curve, yielding the number of converted atoms (red). The data is fitted with solutions to coupled differential equations (solid lines), extracting the lifetimes of each state and the fraction of atoms converted through the aforementioned Raman channel [50]. Error bars correspond to the standard error of the mean of three averages. (b) While the ground-state loss rate benefits from deep lattices, Raman losses lead to a linear increase in the $^3P_0$ clock-state loss rate for lattice depths $\gtrsim 250\,E_{rec}$. Below the optimal trap depth of $220\,E_{rec}$ (white circle), strong inelastic collisions and spilling losses start to become dominant. Error bars from the exponential fit uncertainties are smaller than the datapoints, and the solid lines are exponential fits ($^1S_0$) in combination with a linear term ($^3P_0$).

detuning [Fig. 5(b)]. As can be expected from the negligibly small curvature of the $^3P_0$ polarizability within the tuning range and from simple perturbation theory calculations [35,58], the modulation-induced excess loss rate scales quadratically in Δ [Fig. 5(c)]. However, this simple model breaks down for very fast loss dynamics. Here, we observe the emergence of additional, slower timescales arising in the lifetime curves, where the separation into mostly phase- and amplitude-modulated lattice sites and the strong dependence of tunneling rates on the harmonic oscillator state starts to play a role. We therefore restrict the analysis to data that is well described by a single exponential function and perform each measurement at three different average tune-out lattice powers [29]. Computing the weighted mean of the resulting minima then yields a $^3P_0$ tune-out frequency of

$$f_{to} = 519.9199 \pm 29_{stat} \left(^{+57}_{-45}\right)_{sys} \text{ THz}. \quad (2)$$

Here, the statistical uncertainty corresponds to the standard error of the mean, while for the systematic uncertainty we take the deviation from the perturbative regime into account by fitting both the limited and the full dataset with an empirical function that includes a smooth crossover to a linear regime for large detunings [29]. Notably, since known isotope shifts of relevant transitions are typically on the order of few gigahertz or less, we expect that the tune-out frequencies for other Yb isotopes are within the error bar of f_{to}.

We can compare the measured tune-out wavelength value to the empirical model presented in Ref. [28] and find excellent agreement. Including f_{to} in the model therefore leads to marginal changes of the fit parameters [29]. Leveraging the vanishing $^3P_0$ polarizability at f_{to}, we further measure the ac Stark shift of the ground state by means of high-resolution clock spectroscopy in the presence of a static, unreflected dipole beam at the tune-out wavelength for varying powers. Repeating this measurement after tuning the laser to the clock transition enables a direct comparison of the relative light shift ratio, which we quantify to be $\Delta\alpha_{to}/\Delta\alpha_{clock} = 1.014(11)$. Together with the previously determined clock probe shift of $15(3)\,\text{Hz}/(\text{W}/\text{cm}^2)$ reported in Ref. [59], we thus find the empirical model's prediction for the $^1S_0$ polarizability at the tune-out wavelength of $V_{ac}/I = -13.0\,h\,\text{Hz}/(\text{W}/\text{cm}^2)$ to be well within the error bar.

Notably, the presence of the tune-out beam leads to enhanced losses from off-resonant Raman processes, which however do not vary over the chosen detuning range and thus yield a constant offset to the lifetime in the bare 2D lattice. Utilizing the light shift measurement reported above as an intensity calibration [29], we measure the Raman loss rate to be $12(3) \times 10^{-6}\,\text{Hz}/(\text{W}/\text{cm}^2)$, which reasonably agrees with a theoretical estimate of $10.2 \times 10^{-6}\,\text{Hz}/(\text{W}/\text{cm}^2)$ [29,50].

III. SUMMARY AND CONCLUSION

In this work we have presented the first measurement of a metastable excited-state tune-out wavelength, aided by a combination of sideband cooling on the $^1S_0 \to {}^3P_0$ and molasses cooling on the $^1S_0 \to {}^3P_1$ transition. For the latter, we have identified a novel magic angle that allows for triple-magic operation at 759 nm trap light with bosonic ^{174}Yb atoms and characterized a stability region of effective cooling during fluorescence imaging in a 3D clock-magic lattice. This represents a major step towards the realization of an Yb quantum gas microscope with a clock-magic lattice, while the newly determined tune-out wavelength greatly enriches the toolbox for applications in quantum computing and simulation. In particular, tune-out wavelengths may be beneficial for rearrangement of atoms in dense arrays or lattices. Here, one can utilize the ability to apply local light shifts to selectively shelve atoms to the metastable clock state with minimal impact on their coherence as well as to shuttle ground-state atoms to the desired final position without disturbing the potential of shelved atoms, enhancing the scalability of existing quantum computation schemes [1,20,49]. Moreover, the triple-magic

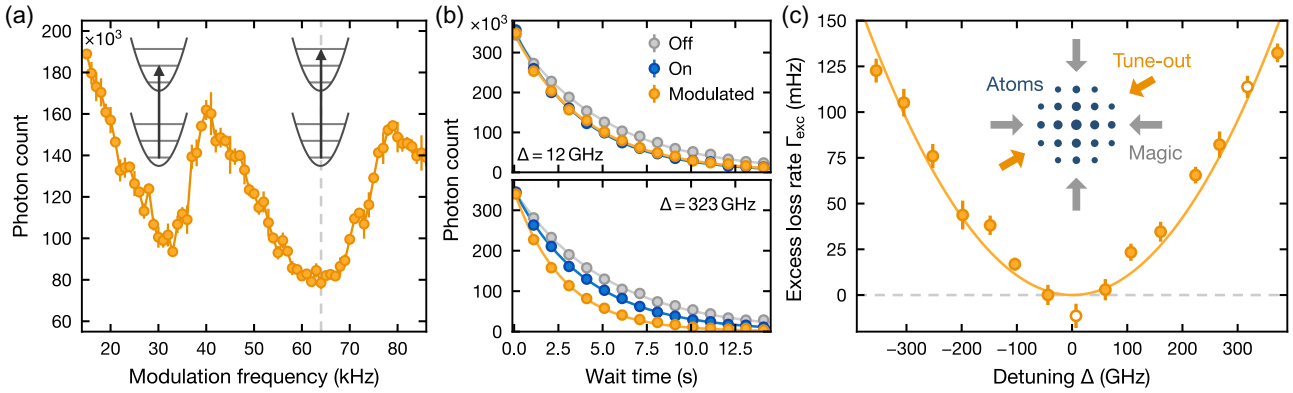


FIG. 5. Determination of the $^3P_0$ clock-state tune-out wavelength. (a) Modulation spectroscopy of clock-state atoms approximately 1 THz detuned from the tune-out wavelength. After 1.5 s of intensity modulation, strong loss features can be found at the longitudinal trap frequency of ≈ 32 kHz and its first multiple, with the former corresponding to excitations by one and the latter by two harmonic oscillator quanta (insets). The solid line is a linear interpolation. (b) Clock-state lifetimes in the bare clock-magic lattice (gray), with the additional tune-out lattice at constant amplitude (blue), and with intensity modulation of the tune-out lattice at $f_{\mathrm{mod}} = 64$ kHz [orange, gray dotted line in (a)]. While the presence of the tune-out lattice induces a moderate, constant excess loss, its modulation leads to pronounced losses for large detunings Δ from the tune-out wavelength (bottom panel) and does not affect the lifetime close to it (top panel). We fit the data with single exponential functions (solid lines). The error bars obtained from three averages are smaller than the datapoints. (c) Excess loss rate from modulation compared to the static tune-out lattice case for varying laser frequencies [white markers indicate the parameters used for the measurements in (b)]. The data follows a quadratic trend (solid line). The error bars are obtained from the standard deviation of the individual lifetime fit uncertainties. Inset: sketch of the total lattice geometry, with the tune-out lattice at an arbitrarily chosen angle of 30° with respect to the magic 2D lattice.

condition for $^3P_1$ and $^3P_0$ in a short-spacing retro-reflected lattice offers exciting opportunities for the realization of novel light-matter interfaces in extreme sub-wavelength arrays [60–62].

ACKNOWLEDGMENTS

We thank Etienne Staub for experimental assistance. This project has received funding from the Deutsche Forschungsgemeinschaft (DFG, German Research Foundation) under Germany's Excellence Strategy – EXC-2111 – 390814868 and via Research Unit FOR5522 under Project No. 499180199. We further acknowledge funding from the European Research Council (ERC) under the European Union's Horizon 2020 research and innovation program (Grant Agreement No. 803047), from the German Federal Ministry of Education and Research (BMBF) via the funding program quantum technologies – from basic research to market (Contract No. 13N15895 FermiQP) and from the Initiative *Munich Quantum Valley* from the State Ministry for Science and the Arts as part of the High-Tech Agenda Plus of the Bavarian State Government. This work has further received funding under Horizon Europe programme HORIZON-CL4-2022-QUANTUM-02-SGA via the Project 101113690 (PASQuanS2.1) and from the European Union's Horizon 2020 research and innovation programme under Grant Agreement No. 101017733 (DYNAMITE, DFG Project No. 499183856).

DATA AVAILABILITY

The data that support the findings of this article are openly available [63].

[1] J. W. Lis, A. Senoo, W. F. McGrew, F. Rönchen, A. Jenkins, and A. M. Kaufman, Midcircuit operations using the *omg* architecture in neutral atom arrays, Phys. Rev. X **13**, 041035 (2023).

[2] S. Ma, G. Liu, P. Peng, B. Zhang, S. Jandura, J. Claes, A. P. Burgers, G. Pupillo, S. Puri, and J. D. Thompson, High-fidelity gates and mid-circuit erasure conversion in an atomic qubit, Nature **622**, 279 (2023).

[3] W. Huie, L. Li, N. Chen, X. Hu, Z. Jia, WonKyuCalvin Sun, and J. P. Covey, Repetitive readout and real-time control of nuclear spin qubits in ^{171}Yb atoms, PRX Quantum **4**, 030337 (2023).

[4] B. W. Reichardt *et al.*, Fault-tolerant quantum computation with a neutral atom processor, ArXiv:2411.11822.

[5] F. Scazza, C. Hofrichter, M. Höfer, P. C. De Groot, I. Bloch, and S. Fölling, Observation of two-orbital spin-exchange interactions with ultracold SU(N)-symmetric fermions, Nat. Phys. **10**, 779 (2014).

[6] G. Pagano, M. Mancini, G. Cappellini, P. Lombardi, F. Schäfer, H. Hu, X.-J. Liu, J. Catani, C. Sias, M. Inguscio, and L. Fallani, A one-dimensional liquid of fermions with tunable spin, Nat. Phys. **10**, 198 (2014).

[7] S. Taie, E. Ibarra-García-Padilla, N. Nishizawa, Y. Takasu, Y. Kuno, H.-T. Wei, R. T. Scalettar, K. R. Hazzard, and Y. Takahashi, Observation of antiferromagnetic correlations in

an ultracold SU(N) Hubbard model, Nat. Phys. **18**, 1356 (2022).

[8] G. Pasqualetti, O. Bettermann, N. Darkwah Oppong, E. Ibarra-García-Padilla, S. Dasgupta, R. T. Scalettar, K. R. A. Hazzard, I. Bloch, and S. Fölling, Equation of state and thermometry of the 2D SU(N) Fermi-Hubbard model, Phys. Rev. Lett. **132**, 083401 (2024).

[9] J. Ye, H. J. Kimble, and H. Katori, Quantum state engineering and precision metrology using state-insensitive light traps, Science **320**, 1734 (2008).

[10] A. D. Ludlow, M. M. Boyd, J. Ye, E. Peik, and P. O. Schmidt, Optical atomic clocks, Rev. Mod. Phys. **87**, 637 (2015).

[11] A. Aeppli, K. Kim, W. Warfield, M. S. Safronova, and J. Ye, Clock with 8×10^{-19} systematic uncertainty, Phys. Rev. Lett. **133**, 023401 (2024).

[12] M. A. Norcia, A. W. Young, W. J. Eckner, E. Oelker, J. Ye, and A. M. Kaufman, Seconds-scale coherence on an optical clock transition in a tweezer array, Science **366**, 93 (2019).

[13] I. S. Madjarov, A. Cooper, A. L. Shaw, J. P. Covey, V. Schkolnik, T. H. Yoon, J. R. Williams, and M. Endres, An atomic-array optical clock with single-atom readout, Phys. Rev. X **9**, 041052 (2019).

[14] A. Cao, W. J. Eckner, T. Lukin Yelin, A. W. Young, S. Jandura, L. Yan, K. Kim, G. Pupillo, J. Ye, N. Darkwah Oppong, and A. M. Kaufman, Multi-qubit gates and Schrödinger cat states in an optical clock, Nature **634**, 315 (2024).

[15] S. Kolkowitz, S. Bromley, T. Bothwell, M. Wall, G. Marti, A. Koller, X. Zhang, A. Rey, and J. Ye, Spin–orbit-coupled fermions in an optical lattice clock, Nature **542**, 66 (2017).

[16] M. Mancini, G. Pagano, G. Cappellini, L. Livi, M. Rider, J. Catani, C. Sias, P. Zoller, M. Inguscio, M. Dalmonte, and L. Fallani, Observation of chiral edge states with neutral fermions in synthetic Hall ribbons, Science **349**, 1510 (2015).

[17] T. W. Zhou, T. Beller, G. Masini, J. Parravicini, G. Cappellini, C. Repellin, T. Giamarchi, J. Catani, M. Filippone, and L. Fallani, Measuring Hall voltage and Hall resistance in an atom-based quantum simulator, ArXiv:2411.09744.

[18] Z. W. Barber, J. E. Stalnaker, N. D. Lemke, N. Poli, C. W. Oates, T. M. Fortier, S. A. Diddams, L. Hollberg, C. W. Hoyt, A. V. Taichenachev, and V. I. Yudin, Optical lattice induced light shifts in an Yb atomic clock, Phys. Rev. Lett. **100**, 103002 (2008).

[19] C. Chen, G. Bornet, M. Bintz, G. Emperauger, L. Leclerc, V. S. Liu, P. Scholl, D. Barredo, J. Hauschild, S. Chatterjee, M. Schuler, A. Läuchli, M. P. Zaletel, T. Lahaye, N. Y. Yao, and A. Browaeys, Continuous symmetry breaking in a two-dimensional Rydberg array, Nature **616**, 691 (2023).

[20] D. Bluvstein *et al.*, Logical quantum processor based on reconfigurable atom arrays, Nature **626**, 58 (2024).

[21] N. Darkwah Oppong, G. Pasqualetti, O. Bettermann, P. Zechmann, M. Knap, I. Bloch, and S. Fölling, Probing transport and slow relaxation in the mass-imbalanced Fermi-Hubbard model, Phys. Rev. X **12**, 031026 (2022).

[22] F. M. Surace, P. Fromholz, N. Darkwah Oppong, M. Dalmonte, and M. Aidelsburger, *Ab initio* derivation of lattice-gauge-theory dynamics for cold gases in optical lattices, PRX Quantum **4**, 020330 (2023).

[23] A. González-Tudela, and J. I. Cirac, Cold atoms in twisted-bilayer optical potentials, Phys. Rev. A **100**, 053604 (2019).

[24] X.-W. Luo, and C. Zhang, Spin-twisted optical lattices: Tunable flat bands and Larkin-Ovchinnikov superfluids, Phys. Rev. Lett. **126**, 103201 (2021).

[25] G. Pagano, F. Scazza, and M. Foss-Feig, Fast and scalable quantum information processing with two-electron atoms in optical tweezer arrays, Adv. Quantum Tech. **2**, 1800067 (2019).

[26] A. J. Daley, M. M. Boyd, J. Ye, and P. Zoller, Quantum computing with alkaline-earth-metal atoms, Phys. Rev. Lett. **101**, 170504 (2008).

[27] D. González-Cuadra, D. Bluvstein, M. Kalinowski, R. Kaubruegger, N. Maskara, P. Naldesi, T. V. Zache, A. M. Kaufman, M. D. Lukin, H. Pichler, B. Vermersch, J. Ye, and P. Zoller, Fermionic quantum processing with programmable neutral atom arrays, Proc. Natl. Acad. Sci. USA **120**, e2304294120 (2023).

[28] T. O. Höhn, E. Staub, G. Brochier, N. Darkwah Oppong, and M. Aidelsburger, State-dependent potentials for the $^1S_0$ and $^3P_0$ clock states of neutral ytterbium atoms, Phys. Rev. A **108**, 053325 (2023).

[29] See Supplemental Material at http://link.aps.org/supplemental/10.1103/32q9-j82c, which includes Refs. [64–69], for additional information about the experimental setup and sequences, the initial state characterization, read-out techniques, additional data and error analysis for the magic angle and tune-out measurements, experimental results on the Raman scattering rate and the differential light shift at f_{to} and at the clock resonance, and a discussion of the expanded empirical polarizability model.

[30] M. S. Safronova, Z. Zuhrianda, U. I. Safronova, and C. W. Clark, Extracting transition rates from zero-polarizability spectroscopy, Phys. Rev. A **92**, 040501(R) (2015).

[31] M. A. Norcia, A. W. Young, and A. M. Kaufman, Microscopic control and detection of ultracold strontium in optical-tweezer arrays, Phys. Rev. X **8**, 041054 (2018).

[32] G. Unnikrishnan, P. Ilzhöfer, A. Scholz, C. Hölzl, A. Götzelmann, R. K. Gupta, J. Zhao, J. Krauter, S. Weber, N. Makki, H. P. Büchler, T. Pfau, and F. Meinert, Coherent control of the fine-structure qubit in a single alkaline-earth atom, Phys. Rev. Lett. **132**, 150606 (2024).

[33] M. Ammenwerth, H. Timme, F. Gyger, R. Tao, I. Bloch, and J. Zeiher, Realization of a fast triple-magic all-optical qutrit in ^{88}Sr, Phys. Rev. Lett. **135**, 143401 (2025).

[34] A. Cooper, J. P. Covey, I. S. Madjarov, S. G. Porsev, M. S. Safronova, and M. Endres, Alkaline-earth atoms in optical tweezers, Phys. Rev. X **8**, 041055 (2018).

[35] A. Heinz, A. J. Park, N. Šantić, J. Trautmann, S. G. Porsev, M. S. Safronova, I. Bloch, and S. Blatt, State-dependent optical lattices for the strontium optical qubit, Phys. Rev. Lett. **124**, 203201 (2020).

[36] L. Franchi, L. F. Livi, G. Cappellini, G. Binella, M. Inguscio, J. Catani, and L. Fallani, State-dependent interactions in ultracold ^{174}Yb probed by optical clock spectroscopy, New J. Phys. **19**, 103037 (2017).

[37] R. Bouganne, M. B. Aguilera, A. Dareau, E. Soave, J. Beugnon, and F. Gerbier, Clock spectroscopy of interacting bosons in deep optical lattices, New J. Phys. **19**, 113006 (2017).

[38] C. D. Herold, V. D. Vaidya, X. Li, S. L. Rolston, J. V. Porto, and M. S. Safronova, Precision measurement of transition matrix elements via light shift cancellation, Phys. Rev. Lett. **109**, 243003 (2012).

[39] A. Ratkata, P. D. Gregory, A. D. Innes, A. J. Matthies, L. A. McArd, J. M. Mortlock, M. S. Safronova, S. L. Bromley, and S. L. Cornish, Measurement of the tune-out wavelength for ^{133}Cs at 880 nm, Phys. Rev. A **104**, 052813 (2021).

[40] F. Schmidt, D. Mayer, M. Hohmann, T. Lausch, F. Kindermann, and A. Widera, Precision measurement of the ^{87}Rb tune-out wavelength in the hyperfine ground state $F = 1$ at 790 nm, Phys. Rev. A **93**, 022507 (2016).

[41] W. Kao, Y. Tang, N. Q. Burdick, and B. L. Lev, Anisotropic dependence of tune-out wavelength near Dy 741-nm transition, Opt. Express **25**, 3411 (2017).

[42] J. Catani, G. Barontini, G. Lamporesi, F. Rabatti, G. Thalhammer, F. Minardi, S. Stringari, and M. Inguscio, Entropy exchange in a mixture of ultracold atoms, Phys. Rev. Lett. **103**, 140401 (2009).

[43] R. M. Kroeze, R. A. Villela, E. Zu, T. O. Höhn, and M. Aidelsburger, Isotope-agnostic motional ground-state cooling of neutral Yb atoms, Phys. Rev. Res. (to be published).

[44] S. Dörscher, R. Schwarz, A. Al-Masoudi, S. Falke, U. Sterr, and C. Lisdat, Lattice-induced photon scattering in an optical lattice clock, Phys. Rev. A **97**, 063419 (2018).

[45] R. Yamamoto, J. Kobayashi, T. Kuno, K. Kato, and Y. Takahashi, An ytterbium quantum gas microscope with narrow-line laser cooling, New J. Phys. **18**, 023016 (2016).

[46] A. Jenkins, J. W. Lis, A. Senoo, W. F. McGrew, and A. M. Kaufman, Ytterbium nuclear-spin qubits in an optical tweezer array, Phys. Rev. X **12**, 021027 (2022).

[47] S. Ma, A. P. Burgers, G. Liu, J. Wilson, B. Zhang, and J. D. Thompson, Universal gate operations on nuclear spin qubits in an optical tweezer array of ^{171}Yb atoms, Phys. Rev. X **12**, 021028 (2022).

[48] M. A. Norcia *et al.*, Midcircuit qubit measurement and rearrangement in a ^{171}Yb atomic array, Phys. Rev. X **13**, 041034 (2023).

[49] M. A. Norcia *et al.*, Iterative assembly of ^{171}Yb atom arrays with cavity-enhanced optical lattices, PRX Quantum **5**, 030316 (2024).

[50] J. L. Siegel, W. F. McGrew, Y. S. Hassan, C.-C. Chen, K. Beloy, T. Grogan, X. Zhang, and A. D. Ludlow, Excited-band coherent delocalization for improved optical lattice clock performance, Phys. Rev. Lett. **132**, 133201 (2024).

[51] J. Ang'ong'a, C. Huang, J. P. Covey, and B. Gadway, Gray molasses cooling of ^{39}K atoms in optical tweezers, Phys. Rev. Res. **4**, 013240 (2022).

[52] A. T. Grier, I. Ferrier-Barbut, B. S. Rem, M. Delehaye, L. Khaykovich, F. Chevy, and C. Salomon, Λ-enhanced sub-Doppler cooling of lithium atoms in D_1 gray molasses, Phys. Rev. A **87**, 063411 (2013).

[53] A. M. Kaufman, B. J. Lester, and C. A. Regal, Cooling a single atom in an optical tweezer to its quantum ground state, Phys. Rev. X **2**, 041014 (2012).

[54] J. D. Thompson, T. G. Tiecke, A. S. Zibrov, V. Vuletić, and M. D. Lukin, Coherence and Raman sideband cooling of a single atom in an optical tweezer, Phys. Rev. Lett. **110**, 133001 (2013).

[55] S. E. Hamann, D. L. Haycock, G. Klose, P. H. Pax, I. H. Deutsch, and P. S. Jessen, Resolved-sideband Raman cooling to the ground state of an optical lattice, Phys. Rev. Lett. **80**, 4149 (1998).

[56] A. J. Kerman, *Raman sideband cooling and cold atomic collisions in optical lattices*, Ph.D. thesis, Stanford University, California, 2002.

[57] N. Nemitz, T. Ohkubo, M. Takamoto, I. Ushijima, M. Das, N. Ohmae, and H. Katori, Frequency ratio of Yb and Sr clocks with 5×10^{-17} uncertainty at 150 seconds averaging time, Nat. Photon. **10**, 258 (2016).

[58] T. A. Savard, K. M. O'Hara, and J. E. Thomas, Laser-noise-induced heating in far-off resonance optical traps, Phys. Rev. A **56**, R1095 (1997).

[59] N. Poli, Z. W. Barber, N. D. Lemke, C. W. Oates, L. S. Ma, J. E. Stalnaker, T. M. Fortier, S. A. Diddams, L. Hollberg, J. C. Bergquist, A. Brusch, S. Jefferts, T. Heavner, and T. Parker, Frequency evaluation of the doubly forbidden $^1S_0 \rightarrow {}^3P_0$ transition in bosonic ^{174}Yb, Phys. Rev. A **77**, 050501(R) (2008).

[60] L. Henriet, J. S. Douglas, D. E. Chang, and A. Albrecht, Critical open-system dynamics in a one-dimensional optical-lattice clock, Phys. Rev. A **99**, 023802 (2019).

[61] R. Bekenstein, I. Pikovski, H. Pichler, E. Shahmoon, S. F. Yelin, and M. D. Lukin, Quantum metasurfaces with atom arrays, Nat. Phys. **16**, 676 (2020).

[62] S. J. Masson, J. P. Covey, S. Will, and A. Asenjo-Garcia, Dicke superradiance in ordered arrays of multilevel atoms, PRX Quantum **5**, 010344 (2024).

[63] T. O. Höhn, R. A. Villela, E. Zu, L. Bezzo, R. M. Kroeze, and M. Aidelsburger, Data for: Determining the 3P0 excited-state tune-out wavelength of 174Yb in a triple-magic lattice (2025), Edmond, V2, https://doi.org/10.17617/3.72JC1R.

[64] L. Riegger, N. Darkwah Oppong, M. Höfer, D. R. Fernandes, I. Bloch, and S. Fölling, Localized magnetic moments with tunable spin exchange in a gas of ultracold fermions, Phys. Rev. Lett. **120**, 143601 (2018).

[65] D. A. Steck, http://steck.us/teaching Quantum and Atom Optics (2007).

[66] S. G. Porsev, Y. G. Rakhlina, and M. G. Kozlov, Electric-dipole amplitudes, lifetimes, and polarizabilities of the low-lying levels of atomic ytterbium, Phys. Rev. A **60**, 2781 (1999).

[67] K. Blagoev, and V. Komarovskii, Lifetimes of levels of neutral and singly ionized lanthanide atoms, At. Data Nucl. Data Tables **56**, 1 (1994).

[68] A. V. Taichenachev, V. I. Yudin, C. W. Oates, C. W. Hoyt, Z. W. Barber, and L. Hollberg, Magnetic field-induced spectroscopy of forbidden optical transitions with application to lattice-based optical atomic clocks, Phys. Rev. Lett. **96**, 083001 (2006).

[69] B. H. Bransden, and C. J. Joachain, *Physics of Atoms and Molecules* (Pearson Education, Prentice Hall, New York, 2003).